nature energy
SUPPLEMENTARY INFORMATION
https://doi.org/10.1038/s41560-020-0584-y
In the format provided by the authors and unedited.

Decoupling electrolytes towards stable and high-energy rechargeable aqueous zinc–manganese dioxide batteries

Cheng Zhong ✉, Bin Liu, Jia Ding, Xiaorui Liu, Yuwei Zhong, Yuan Li, Changbin Sun, Xiaopeng Han, Yida Deng, Naiqin Zhao and Wenbin Hu ✉

Key Laboratory of Advanced Ceramics and Machining Technology (Ministry of Education), Tianjin Key Laboratory of Composite and Functional Materials, School of Materials Science and Engineering, Tianjin University, Tianjin, China. ✉e-mail: cheng.zhong@tju.edu.cn; wbhu@tju.edu.cn

Supplementary Information

Decoupling electrolytes towards stable and high-energy rechargeable aqueous zinc–manganese dioxide batteries

Cheng Zhong,[1*] Bin Liu[1], Jia Ding[1], Xiaorui Liu[1], Yuwei Zhong[1], Yuan Li[1], Changbin Sun[1], Xiaopeng Han[1], Yida Deng[1], Naiqin Zhao[1], and Wenbin Hu[1*]

[1] Key Laboratory of Advanced Ceramics and Machining Technology (Ministry of Education), Tianjin Key Laboratory of Composite and Functional Materials, School of Materials Science and Engineering, Tianjin University, Tianjin 300072, China

[*]e-mail: cheng.zhong@tju.edu.cn; wbhu@tju.edu.cn

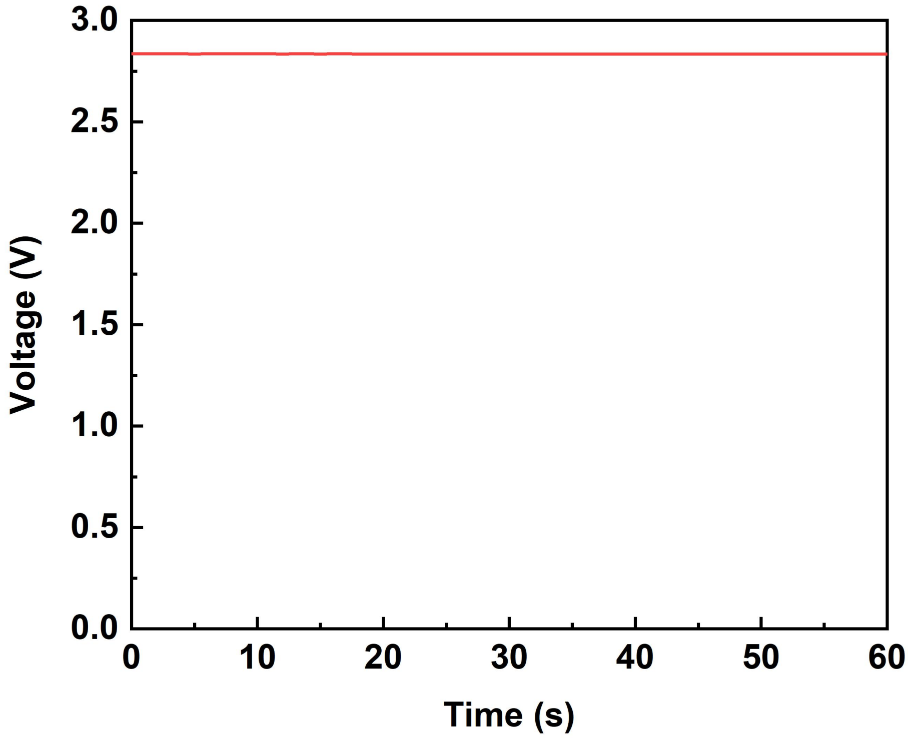

Supplementary Figure 1. Open-circuit voltage measurement of the DZMB. Open-circuit voltage of the DZMB with 3 M H_2SO_4 + 0.1 M $MnSO_4$, 0.1 M K_2SO_4, and 6 M KOH + 0.2 M ZnO + 5 mM vanillin as the acidic solution, neutral solution, and alkaline solution, respectively.

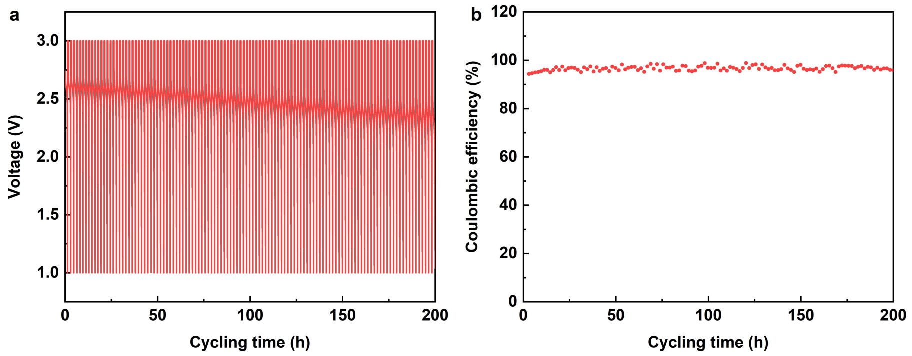

Supplementary Figure 2. Cell performance of the DZMB. a, Discharge and charge curves of the DZMB with a discharge current density of 500 mA g^{-1} and a charge voltage of 3 V and **b,** coulombic efficiency of the DZMB during cycling at a discharge current density of 500 mA g^{-1} and a charge voltage of 3 V.

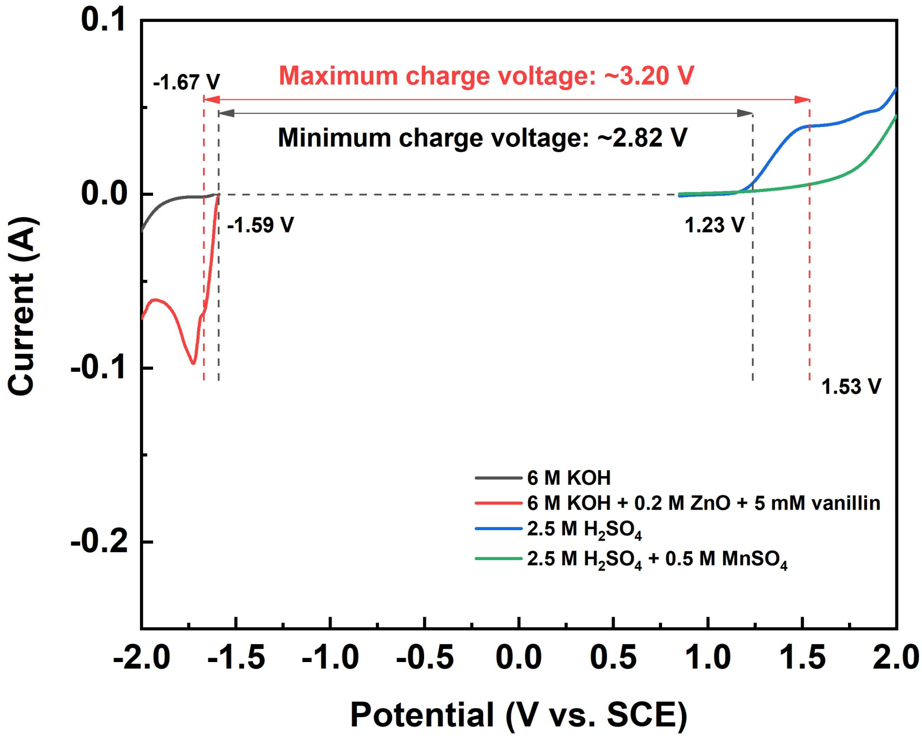

Supplementary Figure 3. Charge voltage determination of the DZMB. As shown in the figure, the minimum charge voltage beyond which MnO_2 and Zn can be successfully deposited is ~2.82 V. The maximum charge voltage is ~3.20 V, which is within the hydrogen evolution reaction (HER) and oxygen evolution reaction (OER) potentials. Therefore, the optimal charge voltage of the DZMB was set to 3.0 V.

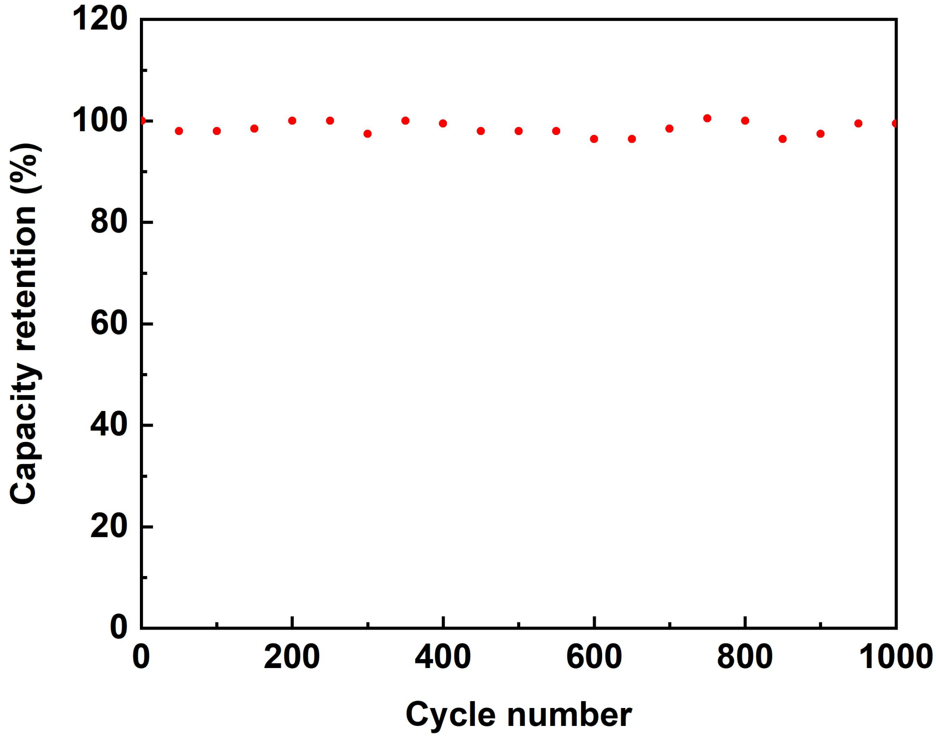

Supplementary Figure 4. Battery capacity retention. Capacity retention of the DZMB with a 10% state of charge at a discharge current density of 1000 mA g^{-1} and a charge voltage of 3 V.

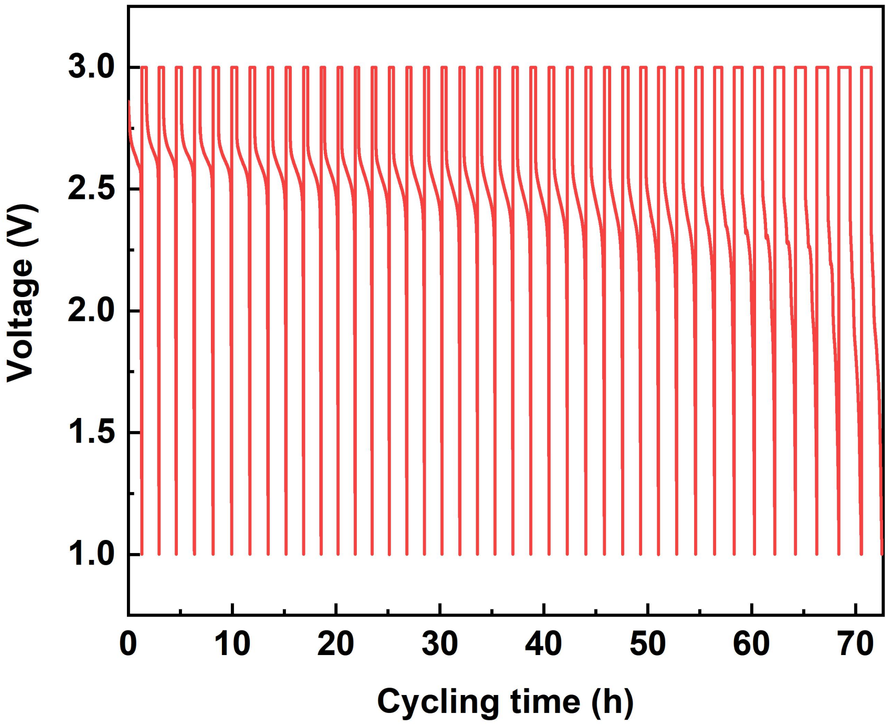

Supplementary Figure 5. Electrochemical performance of Zn–MnO_2 battery with two chambers. Discharge and charge curves of the Zn–MnO_2 battery with an alkaline electrolyte (6 M KOH + 0.2 M ZnO + 5 mM vanillin) and an acidic electrolyte (3 M H_2SO_4 + 0.1 M $MnSO_4$) separated by a cation-exchange membrane with a discharge current density of 500 mA g^{-1} and a charge voltage of 3 V.

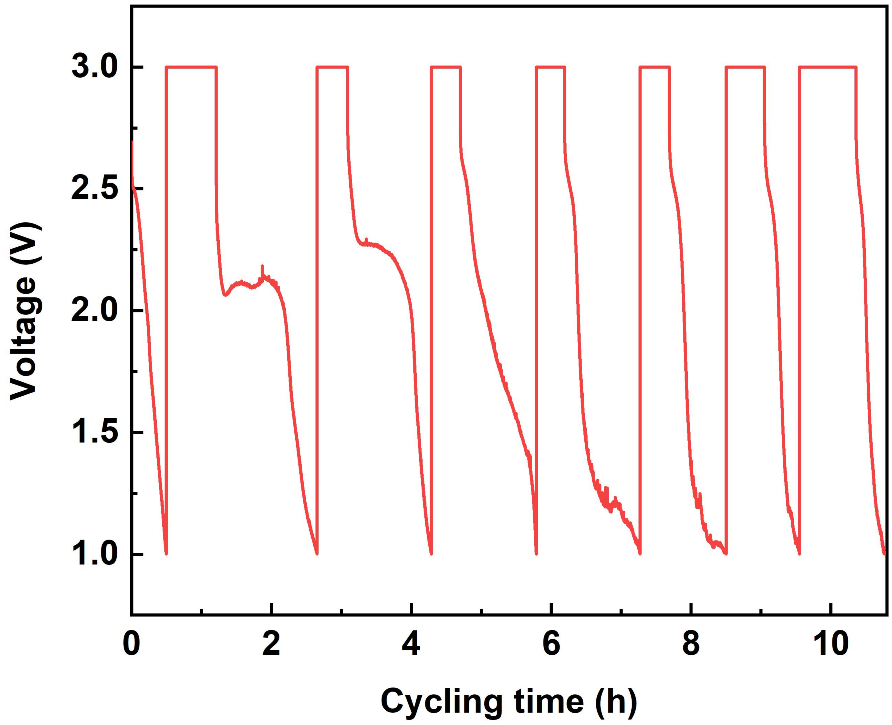

Supplementary Figure 6. Electrochemical performance of Zn–MnO_2 battery with two chambers. Discharge and charge curves of Zn–MnO_2 battery with an alkaline electrolyte (6 M KOH + 0.2 M ZnO + 5 mM vanillin) and an acidic electrolyte (3 M H_2SO_4 + 0.1 M $MnSO_4$) separated by a bipolar membrane with a discharge current density of 500 mA g^{-1} and a charge voltage of 3 V.

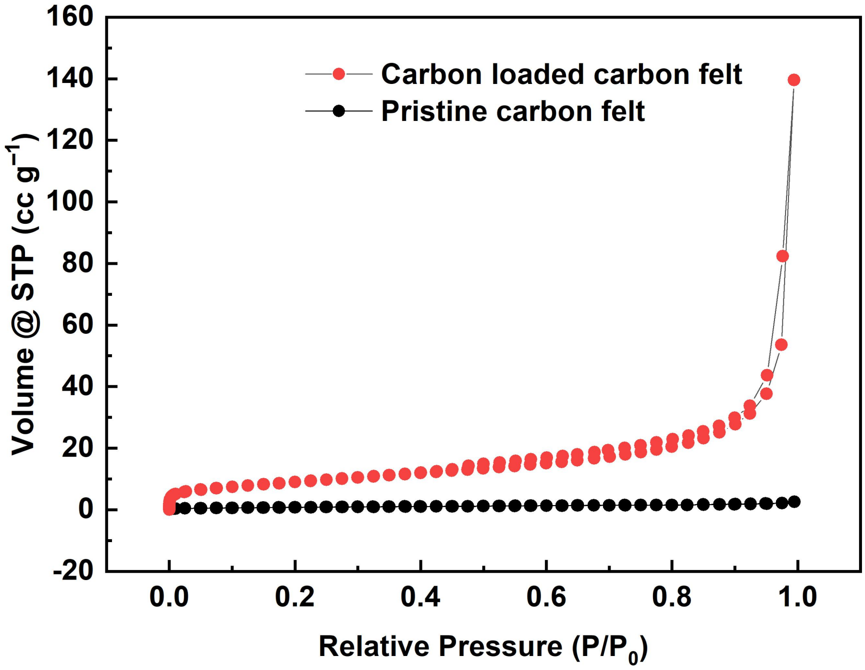

Supplementary Figure 7. Surface area measurement. BET surface area measurement of pristine carbon felt and carbon felt coated with conductive carbon powders.

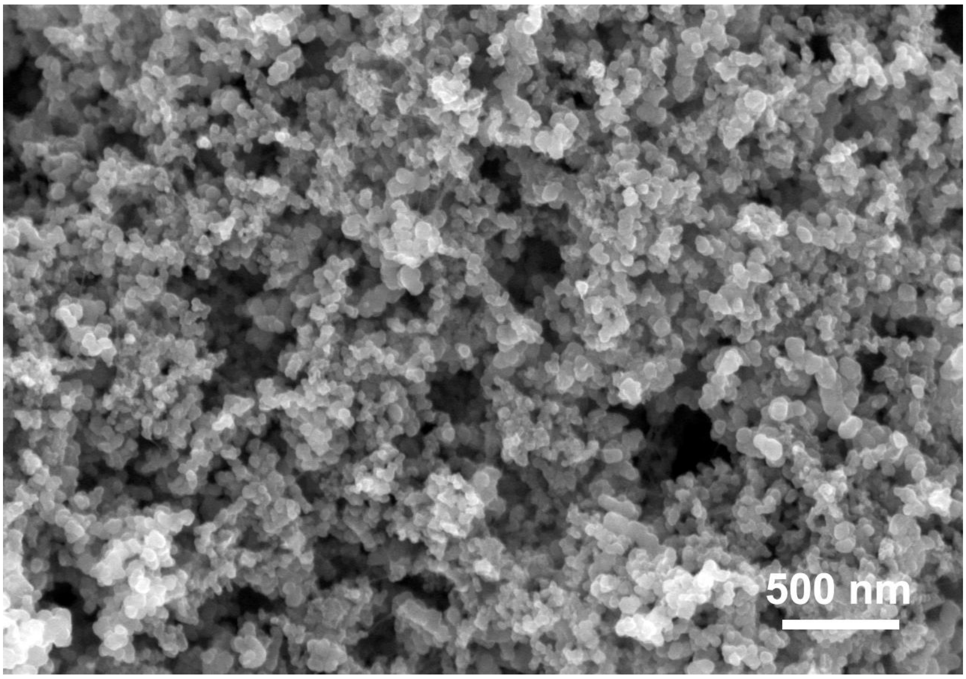

Supplementary Figure 8. SEM characterization. SEM image of the surface morphology of carbon felt loaded with carbon powders.

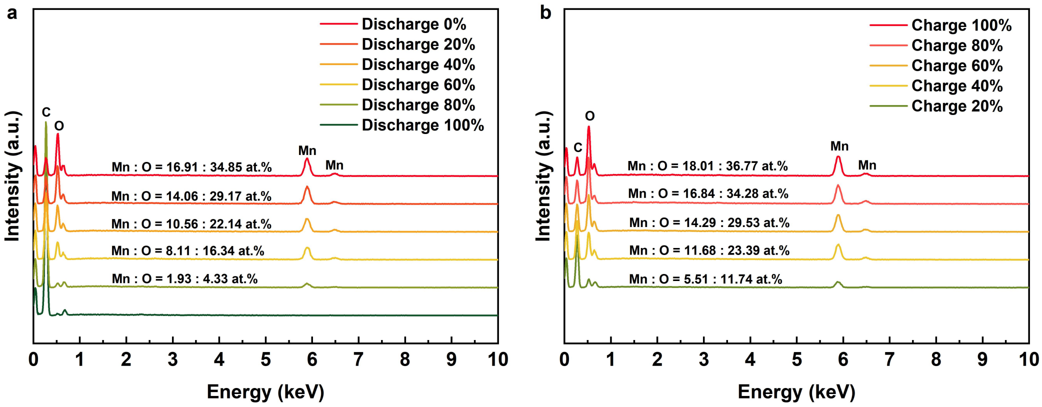

Supplementary Figure 9. Characterization of electrodeposited MnO_2-loaded carbon felt at different states of discharge and charge. a, EDX analysis of the electrodeposited MnO_2-loaded carbon felt at different states of discharge from 0 to 100% and **b,** at different states of charge from 0 to 100%.

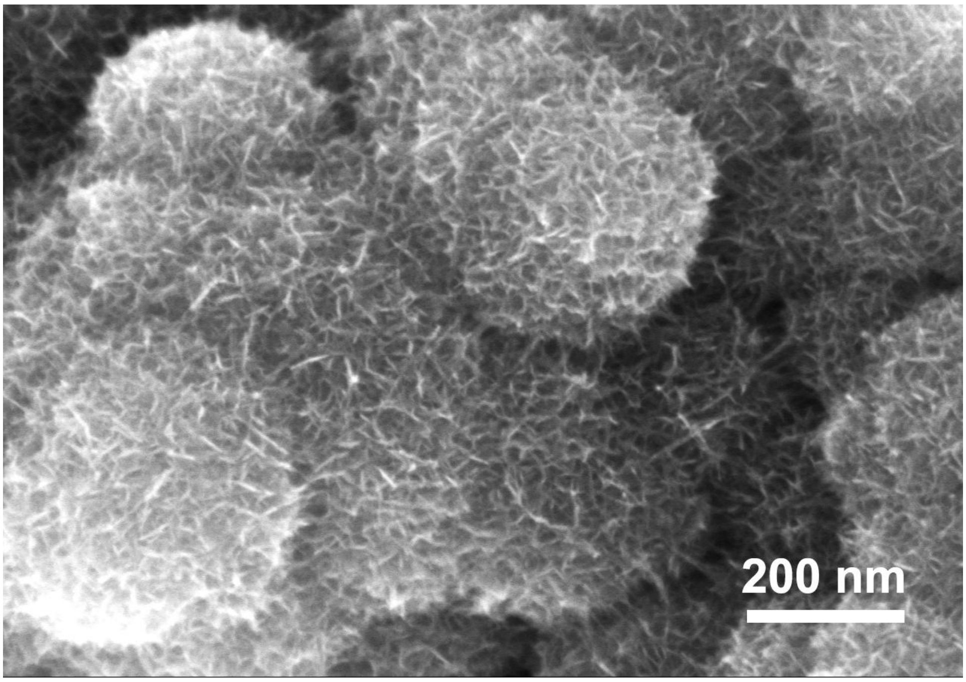

Supplementary Figure 10. SEM characterization. High-magnification SEM image of the surface morphology of electrodeposited MnO_2-loaded carbon felt.

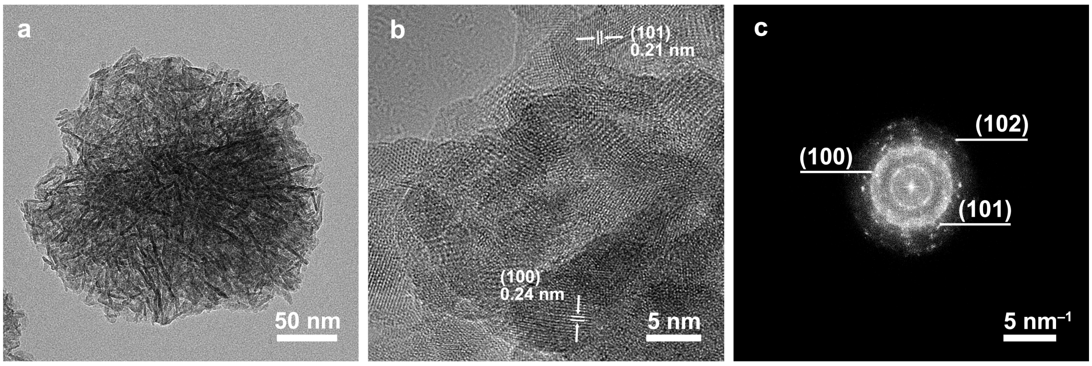

Supplementary Figure 11. Characterization of deposited MnO_2 after the charge. **a,** Low-magnification TEM image and **b,** high-resolution TEM image and **c,** the corresponding FFT pattern of MnO_2 formed on the electrode after the charge process.

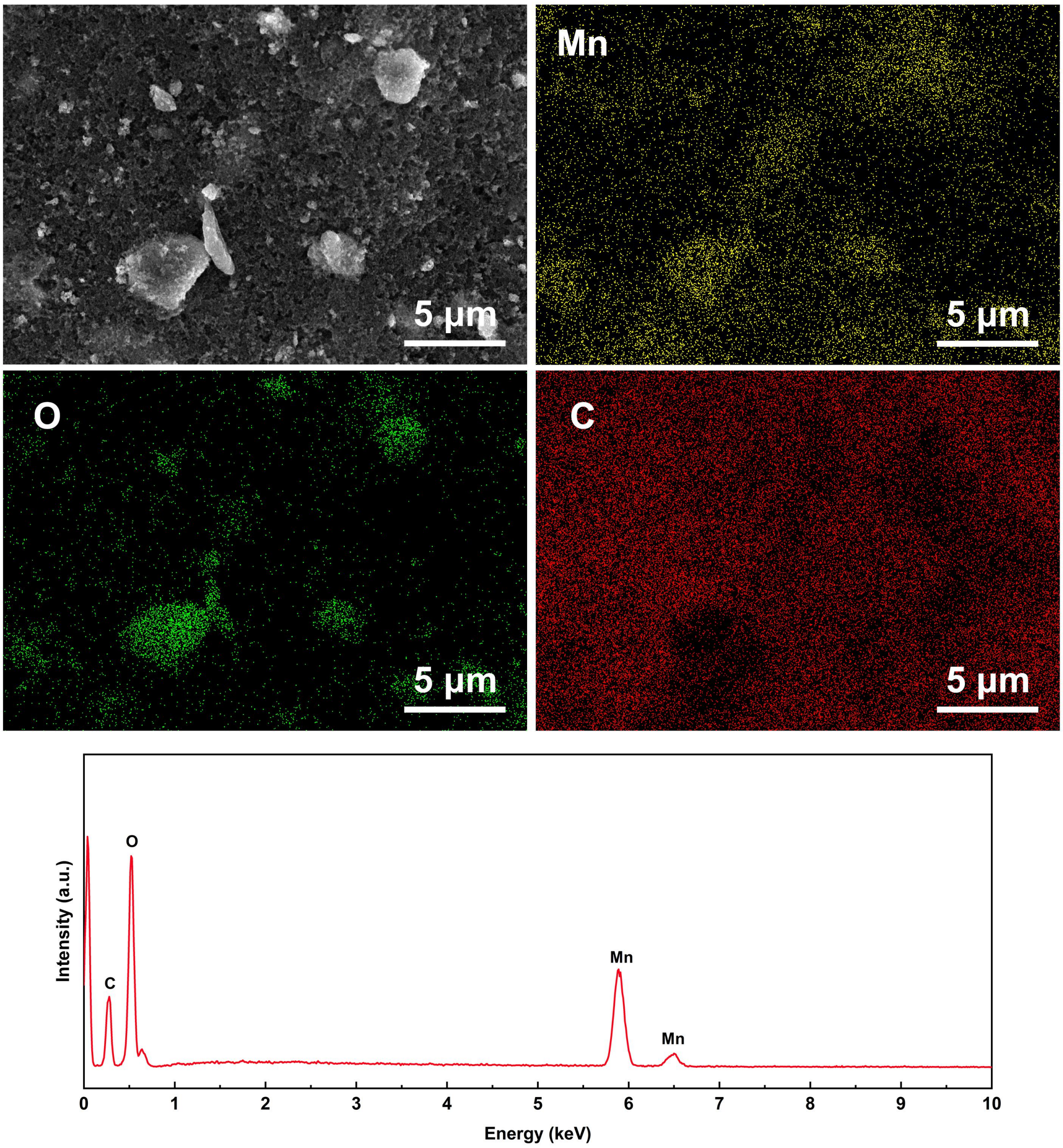

Supplementary Figure 12. Characterization of paste-coated MnO_2 electrode. SEM image of the surface morphology, EDX mapping, and EDX point analysis of the paste-coated MnO_2 electrode using commercial MnO_2 powder.

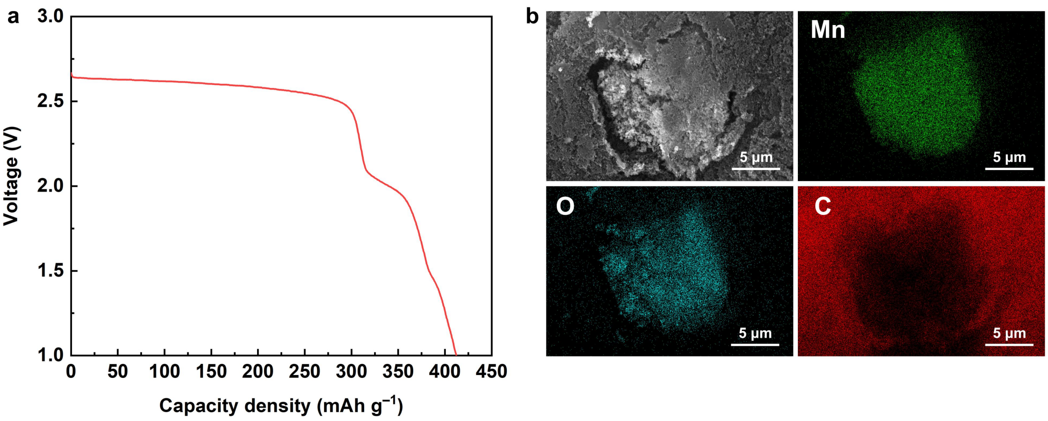

Supplementary Figure 13. Electrochemical performance and characterization of the DZMB based on the paste-coated MnO_2. a, Discharge curve of the DZMB based on the paste-coated MnO_2 electrode at a discharge current density of 500 mA g^{-1}, in which the battery electrolyte was the same as that for the DZMB using the electrodeposited MnO_2 electrode. **b,** SEM image and EDX mapping showing residual MnO_2 particles after the discharge.

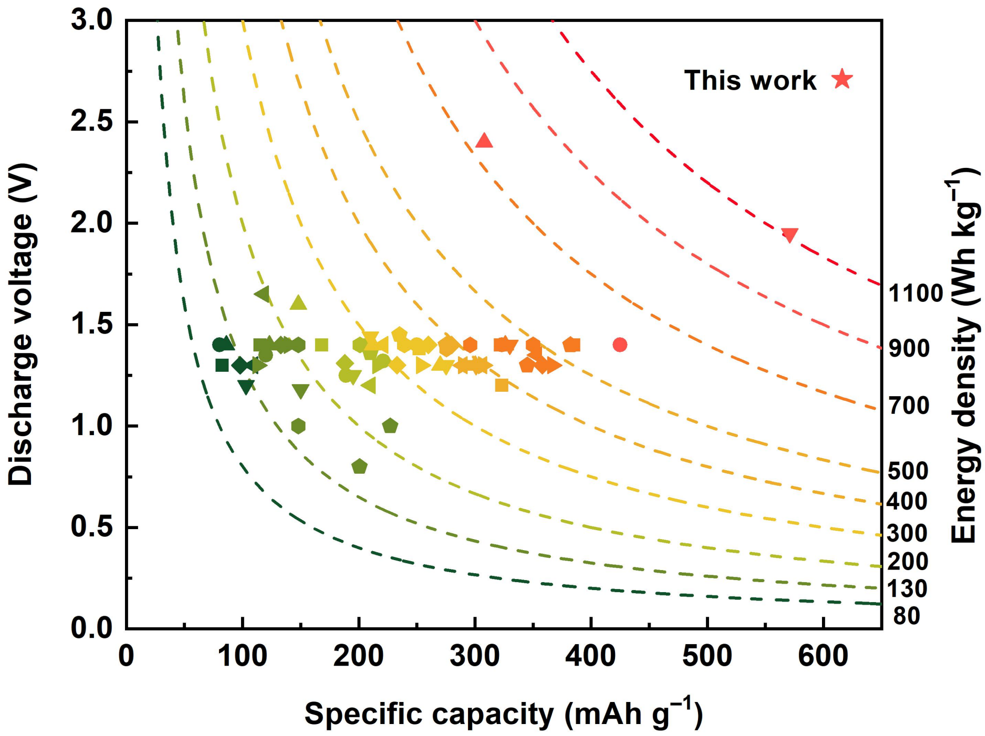

Supplementary Figure 14. Performance comparison. Performance comparison of our scaled-up DZMB with previously reported rechargeable Zn–Mn oxides based batteries (all the discharge voltage and specific capacity data in Supplementary Table 2 were listed, except for the data that were calculated based on the area).

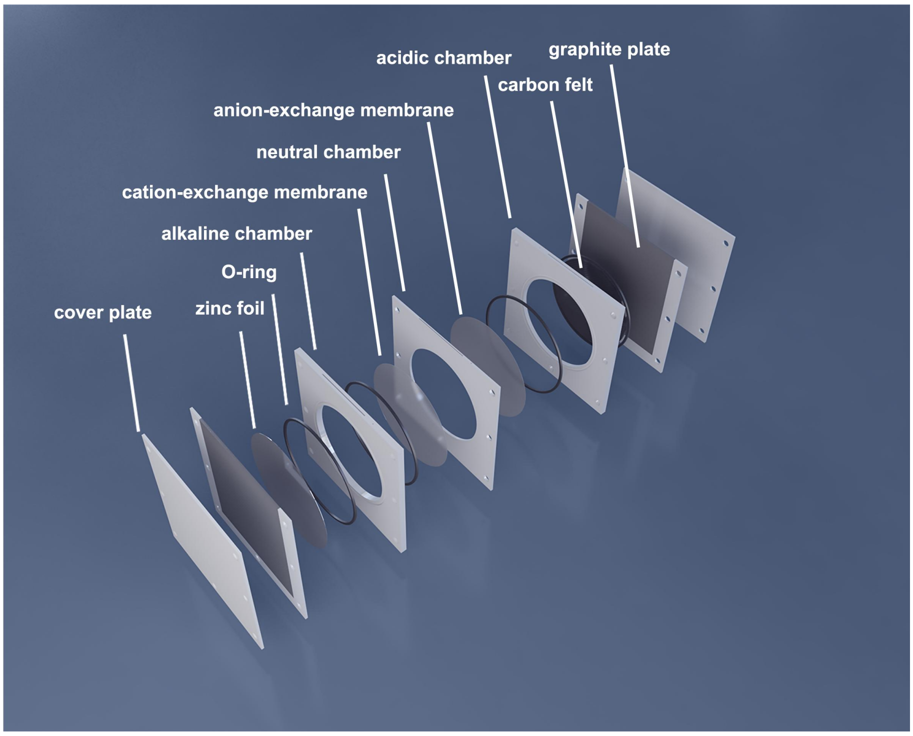

Supplementary Figure 15. Schematic diagram of the DZMB structure.

Supplementary Figure 16. Demonstration of renewable energy storage system. Photos of the renewable energy storage demonstration system based on a DZMB pack (in the middle of the photo) integrated with solar photovoltaic (PV) modules and a wind-driven generator through a controller, and the controller was also connected to a light-emitting diode (LED) panel serving as the electrical load. The floating charge voltage set by the controller was 16 V. The entire system is closed without any external electrical input. Therefore, both the controller and the LED panel are powered by the DZMB pack alone. Due to limitations of the installation location, the natural wind speed was not high enough to charge the battery. Therefore, to effectively test the ability of the DZMB to store both solar and wind energy, an industrial fan was installed to blow the wind-driven generator between the hours of 0:00–4:00.

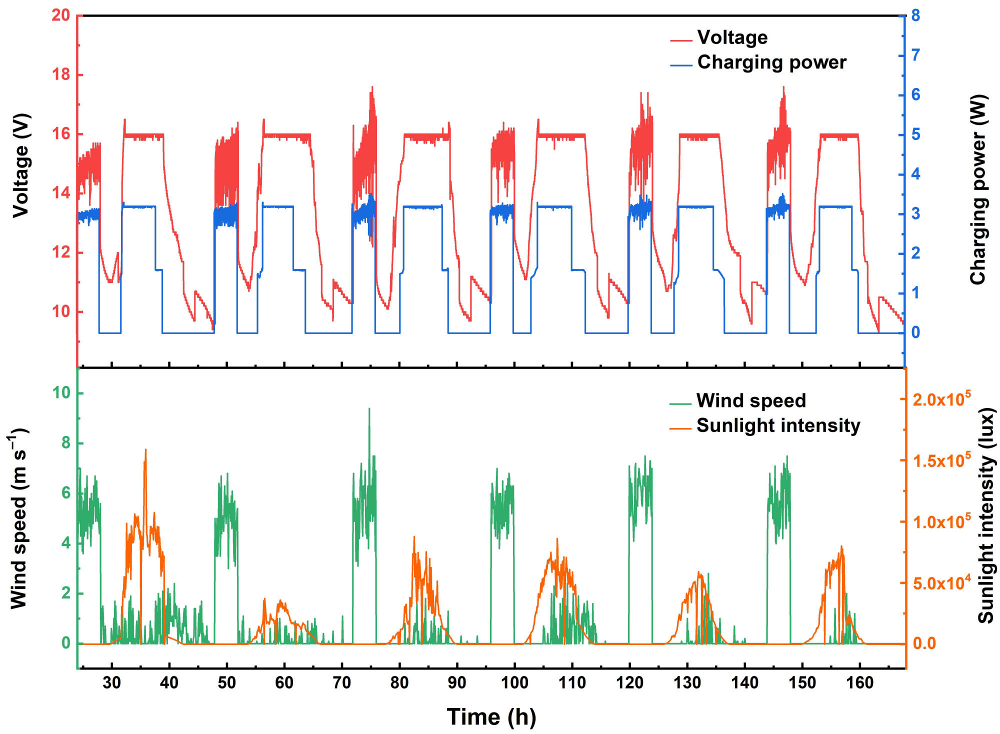

Supplementary Figure 17. Data obtained from the energy storage demonstration system. The voltage and charge power of the DZMB pack, wind speed, and sunlight intensity were collected to demonstrate the practical application of the DZMB in renewable energy storage.

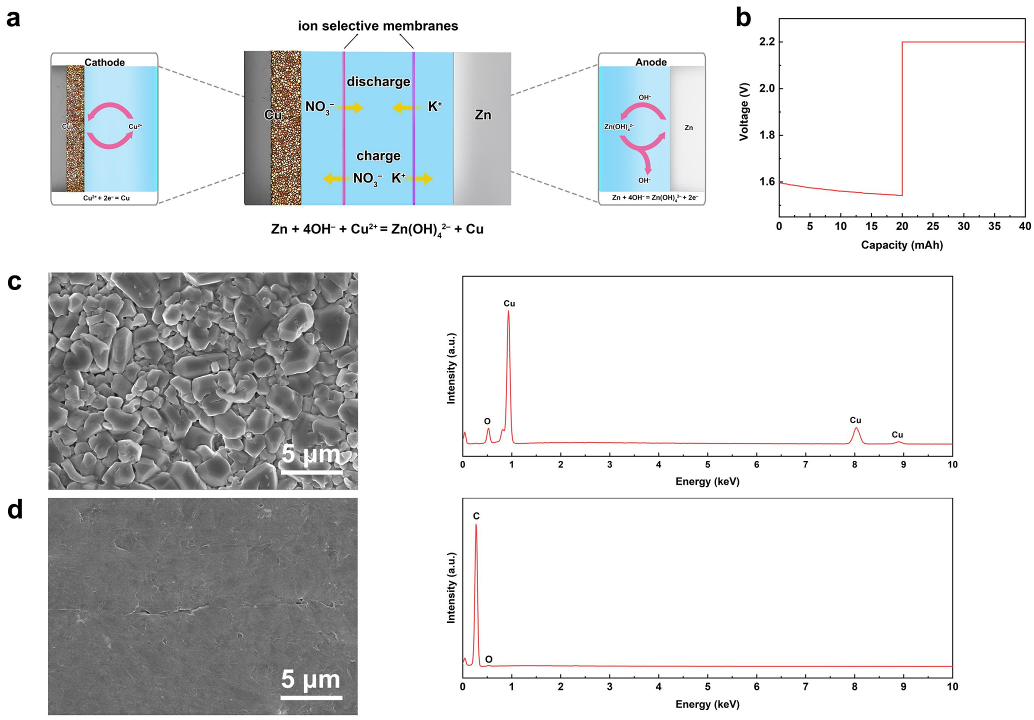

Supplementary Figure 18. Schematic diagram, electrochemical performance, and characterization of decoupled aqueous Zn–Cu battery. a, Schematic diagram of the cell structure and chemical reactions of cathode and anode during the discharge and charge of the decoupled aqueous Zn–Cu battery (DZCB) based on decoupled reactions in acidic and alkaline electrolytes separated by a neutral electrolyte. **b,** Discharge and charge curves of the DZCB based on the acidic electrolyte (1 M $Cu(NO_3)_2$ + 1 M HNO_3), neutral electrolyte (0.1 M KNO_3) and alkaline electrolyte (6 M KOH + 0.2 M ZnO + 5 mM vanillin) at a discharge current of 15 mA and a charge voltage of 2.2 V. **c,** SEM image and EDX analysis of the cathode showing Cu deposits after discharge. **d,** SEM image and EDX analysis of the cathode showing that Cu is completely dissolved after charge.

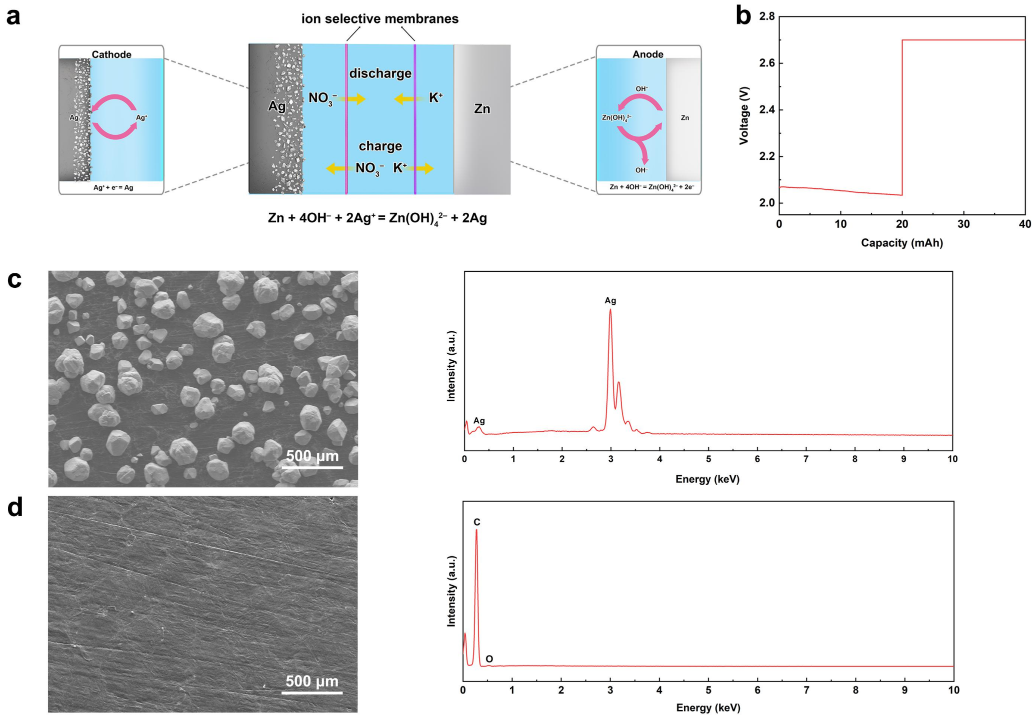

Supplementary Figure 19. Schematic diagram, electrochemical performance, and characterization of decoupled aqueous Zn–Ag battery. a, Schematic diagram of the cell structure and chemical reactions of the cathode and anode during the discharge and charge of the decoupled aqueous Zn–Ag battery (DZAB) based on decoupled reactions in acidic and alkaline electrolytes separated by a neutral electrolyte. **b,** Discharge and charge curves of the DZAB based on the acidic electrolyte (1 M $AgNO_3$ + 1 M HNO_3), neutral electrolyte (0.1 M KNO_3) and alkaline electrolyte (6 M KOH + 0.2 M ZnO + 5 mM vanillin) at a discharge current of 15 mA and a charge voltage of 2.7 V. **c,** SEM image and EDX analysis of the cathode showing Ag deposits after discharge. **d,** SEM image and EDX analysis of the cathode showing that Ag is completely dissolved after charge.

Supplementary Table 1. Summary of the pCOHP analysis for the interaction between unsaturated Mn atom and neighbouring atoms over ε-MnO_2(100) surface with oxygen vacancy.

No.	H* coverage	Mn atom	Neighbouring atom	IpCOHP (eV)	Average IpCOHP (eV)
1	1/12 ML	Mn	O_{1-1}	−1.080	−0.794
			O_{1-2}	−0.561	
			O_{1-3}	−1.211	
			Mn_{1-1}	−0.626	
			Mn_{1-2}	−0.494	
2	3/12 ML	Mn	O_{2-1}	−0.546	−0.790
			O_{2-2}	−1.093	
			O_{2-3}	−1.223	
			Mn_{2-1}	−0.486	
			Mn_{2-2}	−0.602	
3	6/12 ML	Mn	O_{3-1}	−0.344	−0.693
			O_{3-2}	−1.177	
			O_{3-3}	−1.123	
			Mn_{3-1}	−0.340	
			Mn_{3-2}	−0.482	
4	9/12 ML	Mn	Mn_{4-1}	−0.675	−0.529
			Mn_{4-2}	−0.331	
			Mn_{4-3}	−0.713	
			O_{4-1}	−0.395	

Supplementary Table 2. Summary of the comparison of the discharge voltages, specific capacities, specific energy densities, and cell energy densities of aqueous rechargeable Zn–Mn oxides based batteries.

Cathode material	Electrolyte	Discharge voltage	Specific capacity	Specific energy density	Cell energy density[a]	Ref.
MnO_2	6 M KOH + 0.2 M ZnO + 5 mM vanillin‖0.1 M K_2SO_4‖3 M H_2SO_4 + 0.1 M $MnSO_4$	~2.71 V at 100 mA g^{-1}	616 mAh g^{-1} at 100 mA g^{-1}	1621.7 Wh kg^{-1}	* 90 Wh kg^{-1}	This work
MnO_2	1 M $ZnSO_4$ + 1 M $MnSO_4$ + 0.1 M H_2SO_4	1.95 V at 2 mA cm^{-2}	571 mAh g^{-1}	~1100 Wh kg^{-1}	–	1
MnO_2	45 wt.% KOH gelled electrolyte‖ 1 M $MnSO_4$ + 0.5 M H_2SO_4	~2.4 V	308 mAh g^{-1}	–	–	2
MnO_2	0.3 M $ZnSO_4$ + 0.3 M $MnSO_4$	~1.7 V at 4 mA cm^{-2}	~0.8 mAh cm^{-2}	–	–	3
MnO_2	1 M $ZnSO_4$	1.25 V at 10.5 mA g^{-1}	~195 mAh g^{-1} at 10.5 mA g^{-1}	–	–	4
MnO_2	2 M $ZnSO_4$	~1.18 V at 100 mA g^{-1}	~150 mAh g^{-1} at 100 mA g^{-1}	–	–	5
MnO_2	2 M $ZnSO_4$ + 0.1 M $MnSO_4$	1.38 V at 200 mA g^{-1}	275.5 mAh g^{-1} at 200 mA g^{-1}	380.19 Wh kg^{-1} at 200 mA g^{-1}	–	6
MnO_2	1 M $ZnSO_4$	~1.2 V at 16 mA g^{-1}	323 mAh g^{-1} at 16 mA g^{-1}	–	–	7
MnO_2	1 M $ZnSO_4$ + 0.2 M $MnSO_4$	1.4 V at 115 mA g^{-1}	~212 mAh g^{-1} at 115 mA g^{-1}	–	–	8
MnO_2	2 M $ZnSO_4$ + 0.1 M $MnSO_4$	~1.4 V at 300 mA g^{-1}	275.1 mAh g^{-1} at 300 mA g^{-1}	–	–	9
MnO_2	2 M $ZnSO_4$	~1.4 V	~250 mAh g^{-1} at	–	–	10

	+ 0.5 M $MnSO_4$		100 mA g^{-1}			
MnO_2	Polymer gel electrolyte containing KOH	~1.2 V	~210 mAh g^{-1} at 1 mA	–	–	11
MnO_2	2 M $ZnSO_4$ + 0.2 M $MnSO_4$	~1.3 V at 1232 mA g^{-1}	307 mAh g^{-1} at 308 mA g^{-1}	–	–	12
MnO_2	1 M $ZnSO_4$	~1.3 V at 100 mA g^{-1}	289 mAh g^{-1} at 50 mA g^{-1}	–	–	13
MnO_2	EG-waPUA /PAM hydrogel	~1.3 V at 200 mA g^{-1}	275 mAh g^{-1} at 200 mA g^{-1}	–	–	14
MnO_2	1 M $ZnSO_4$	~1.4 V at 100 mA g^{-1}	350 mAh g^{-1} at 100 mA g^{-1}	–	–	15
MnO_2	2 M $ZnSO_4$ + 0.1 M $MnSO_4$	~1.3 V at 30 mA g^{-1}	233 mAh g^{-1} at 30 mA g^{-1}	–	–	16
MnO_2	Zn-alginate/ PAAm	~1.3 V at 110 mA g^{-1}	300.4 mAh g^{-1} at 110 mA g^{-1}	–	–	17
MnO_2	2 M $ZnSO_4$ + 0.4 M $MnSO_4$	~1.3 V at 2 mA cm^{-2}	0.31 mAh cm^{-2} at 2 mA cm^{-2}	154.3 Wh kg^{-1}	–	18
MnO_2	HPG + 6 M KOH	~1 V	~148 mAh g^{-1}	–	–	19
MnO_2	2 M $ZnCl_2$ + 0.4 M $MnSO_4$	~1.35 V	353 mAh g^{-1} at 500 mA g^{-1}	469 Wh kg^{-1} at 500 mA g^{-1}	–	20
MnO_2	2 M $ZnSO_4$ + 0.1 M $MnSO_4$	~1.3 V at 500 mA g^{-1}	253.8 mAh g^{-1} at 500 mA g^{-1}	–	–	21
MnO_2	2 M $ZnSO_4$ + 0.1 M $MnSO_4$	~1.3 V at 300 mA g^{-1}	358 mAh g^{-1} at 300 mA g^{-1}	397 Wh kg^{-1}	–	22
MnO_2	2 M $ZnSO_4$ + 0.2 M $MnSO_4$	~1.3 V	290 mAh g^{-1} at 90 mA g^{-1}	–	–	23
MnO_2	Saturated LiOH + 1 M $ZnSO_4$	1.6 V	148 mAh g^{-1}	–	–	24
	7 M KOH	1.4 V	330 mAh g^{-1}	–	–	
α-MnO_2	2 M $ZnSO_4$	~1.44 V at 61.6 mA g^{-1}	210 mAh g^{-1} at 61.6 mA g^{-1}	–	–	25

α-MnO_2	0.1 M $ZnSO_4$	~1.2 V at 300 mA g^{-1}	103 mAh g^{-1} at 300 mA g^{-1}	–	–	26
α-MnO_2	1 M $ZnSO_4$ + 0.1 M $MnSO_4$	~1.4 V at 246 mA g^{-1}	168 mAh g^{-1} at 246 mA g^{-1}	–	–	27
β-MnO_2	1 M $ZnSO_4$ + 0.1 M $MnSO_4$	~1.3 V at 100 mA g^{-1}	98 mAh g^{-1} at 100 mA g^{-1}	–	–	28
β-MnO_2	1 M $ZnSO_4$	~1.3 V at 100 mA g^{-1}	270 mAh g^{-1} at 100 mA g^{-1}	–	–	29
β-MnO_2	3 M $ZnSO_4$ + 0.1 M $MnSO_4$	~1.4 V at 100 mA g^{-1}	326 mAh g^{-1} at 100 mA g^{-1}	–	–	30
δ-MnO_2	1 M $ZnSO_4$ + 0.1 M $MnSO_4$	~1.4 V at 100 mA g^{-1}	133 mAh g^{-1} at 100 mA g^{-1}	–	–	31
MnO_2@CNT	2 M $ZnCl_2$	~1.4 V at 100 mA g^{-1}	322 mAh g^{-1} at 100 mA g^{-1}	437 Wh kg^{-1}	–	32
MnO_2/CNT	2 M $ZnSO_4$	~1.4 V at 31 mA g^{-1}	201 mAh g^{-1} at 31 mA g^{-1}	–	–	33
α-MnO_2@In_2O_3	2 M $ZnSO_4$ + 0.1 M $MnSO_4$	~1.4 V at 100 mA g^{-1}	425 mAh g^{-1} at 100 mA g^{-1}	–	–	34
MnO_2@PEDOT	PVA/LiCl–$ZnCl_2$–$MnSO_4$ gel	~1.3 V at 740 mA g^{-1}	366.6 mAh g^{-1} at 740 mA g^{-1}	504.9 Wh kg^{-1}	34 Wh kg^{-1}	35
MnO_2@ZHS	2 M $ZnSO_4$ + 0.24 M $MnSO_4$	~1.4 V at 12 mA g^{-1}	123.2 mAh g^{-1}	–	–	36
α-MnO_2@C	1 M $ZnSO_4$	~1.25 V at 66 mA g^{-1}	189 mAh g^{-1} at 66 mA g^{-1}	–	–	37
α-MnO_2/CNT HMs	2 M $ZnSO_4$ + 0.1 M $MnSO_4$	~1.4 V at 200 mA g^{-1}	296 mAh g^{-1} at 200 mA g^{-1}	0.98 Wh cm^{-2}	–	38
α-MnO_2 NFs	2 M $ZnSO_4$ + 0.1 M $MnSO_4$	~1.4 V at 200 mA g^{-1}	260 mAh g^{-1} at 200 mA g^{-1}	0.85 Wh cm^{-2}	–	
γ-MnO_2/graphene	2 M $ZnSO_4$ + 0.4 M $MnSO_4$	~1.3 V at 1 mA cm^{-2}	301 mAh g^{-1} at 500 mA g^{-1}	411.6 Wh kg^{-1} at 500 mA g^{-1}	–	39
δ-MnO_2 /graphite	1 M $ZnSO_4$	1.45 V at 200 mA g^{-1}	235 mAh g^{-1} at 200 mA g^{-1}	–	–	40
CNT/MnO_2/PEDO	PVA/$ZnCl_2$/$MnSO_4$	~1.3 V	306.1 mAh g^{-1} at 1100 mA g^{-1}	379.4 Wh kg^{-1}	–	41

T						
Graphene scroll-coated α-MnO_2	2 M $ZnSO_4$ + 0.2 M $MnSO_4$	~1.4 V at 300 mA g^{-1}	382.2 mAh g^{-1} at 300 mA g^{-1}	406.6 Wh kg^{-1} at 300 mA g^{-1}	–	42
Layered δ-MnO_2	1 M $ZnSO_4$	~1.38 V at 83 mA g^{-1}	252 mAh g^{-1} at 83 mA g^{-1}	–	–	43
$Na_{0.44}MnO_2$	6 M NaOH	~1.4 V at 60.5 mA g^{-1}	80.2 mAh g^{-1} at 60.5 mA g^{-1}	–	–	44
Oxygen-deficient MnO_2	1 M $ZnSO_4$ + 0.2 M $MnSO_4$	~1.3 V	345 mAh g^{-1} at 200 mA g^{-1}	470 Wh kg^{-1}	–	45
PANI-intercalated MnO_2	2 M $ZnSO_4$ + 0.1 M $MnSO_4$	~1.36 V at 50 mA g^{-1}	~210 mAh g^{-1} at 50 mA g^{-1}	–	–	46
ZnHCF@MnO_2	$ZnSO_4$/PVA	~1.65 V at 100 mA g^{-1}	118 mAh g^{-1} at 100 mA g^{-1}	149 Wh kg^{-1}	–	47
α-$K_{0.19}MnO_2$	3 M $Zn(CF_3SO_3)_2$ + 0.2 M $Mn(CF_3SO_3)_2$	~1.3 V at 308 mA g^{-1}	113 mAh g^{-1} at 6.16 A g^{-1}	380 Wh kg^{-1}	–	48
Mn_2O_3	2 M $ZnSO_4$ + 0.1 M $MnSO_4$	~1.4 V at 100 mA g^{-1}	~140 mAh g^{-1} at 100 mA g^{-1}	–	–	49
Mn_2O_3	2 M $ZnSO_4$	~1.4 V at 100 mA g^{-1}	148 mAh g^{-1}	–	–	50
Mn_3O_4	1 M $ZnSO_4$ + 1 M $MnSO_4$	1.32 V at 100 mA g^{-1}	221 mAh g^{-1} at 100 mA g^{-1}	288 Wh kg^{-1} at 100 mA g^{-1}	–	51
Mn_3O_4	2 M $ZnSO_4$	~1.4 V at 100 mA g^{-1}	239.2 mAh g^{-1} at 100 mA g^{-1}	–	–	52
Mn_3O_4@C	2 M $ZnSO_4$ + 0.1 M $MnSO_4$	~1.4 V at 100 mA g^{-1}	323.2 mAh g^{-1} at 100 mA g^{-1}	429.8 Wh kg^{-1} at 100 mA g^{-1}	–	53
Mn_3O_4@NC	2 M $ZnSO_4$ + 0.1 M $MnSO_4$	~1.4 V at 100 mA g^{-1}	280 mAh g^{-1} at 100 mA g^{-1}	–	–	54
MnO_x@N-C	$ZnSO_4$ + $MnSO_4$	~1.4 V at 100 mA g^{-1}	385 mAh g^{-1} at 100 mA g^{-1}	–	–	55
$MgMn_2O_4$	1 M $MgSO_4$ + 1 M $ZnSO_4$ + 0.1 M $MnSO_4$	~1.3 V at 500 mA g^{-1}	109 mAh g^{-1} at 500 mA g^{-1}	370 Wh kg^{-1}	–	56

$ZnMn_2O_4$	1 M $ZnSO_4$ + 0.05 M $MnSO_4$	~1.4 V at 100 mA g^{-1}	86 mAh g^{-1} at 100 mA g^{-1}	–	–	57
$ZnMn_2O_4$/C	3 M $Zn(CF_3SO_3)_2$	1.35 V at 50 mA g^{-1}	120 mAh g^{-1} at 50 mA g^{-1}	~202 Wh kg^{-1}	** 70 Wh kg^{-1}	58
$ZnMn_2O_4$/Mn_2O_3	1 M $ZnSO_4$	~1.3 V at 100 mA g^{-1}	82.6 mAh g^{-1} at 500 mA g^{-1}	–	–	59
$ZnMn_2O_4$/NG	1 M $ZnSO_4$ + 0.05 M $MnSO_4$	~1.4 V at 100 mA g^{-1}	221 mAh g^{-1} at 100 mA g^{-1}	–	–	60
$ZnMn_2O_4$	1 M $ZnSO_4$ + 0.05 M $MnSO_4$	~0.8 V at 200 mA g^{-1}	200.7 mAh g^{-1} at 200 mA g^{-1}	–	*** 81 Wh kg^{-1}	61
rGO@HM-$ZnMn_2O_4$	1 M $ZnSO_4$ + 0.05 M $MnSO_4$	1.31 V at 300 mA g^{-1}	188 mAh g^{-1} at 300 mA g^{-1}	–	–	62
HfO_2-coated ZVO	1 M $ZnSO_4$	~1 V	227 mAh g^{-1} at 100 mA g^{-1}	–	–	63
$K_{0.8}Mn_8O_{16}$	2 M $ZnSO_4$ + 0.1 M $MnSO_4$	~1.3 V at 100 mA g^{-1}	216 mAh g^{-1} at 100 mA g^{-1}	398 Wh kg^{-1}	–	64
$Ni_xMn_{3-x}O_4$ with *in-situ* coated carbon	2 M $ZnSO_4$ + 0.15 M $MnSO_4$	~1.4 V at 150 mA g^{-1}	115 mAh g^{-1} at 150 mA g^{-1}	~178.1 Wh kg^{-1}	** 67 Wh kg^{-1}	65
OD-ZMO @PEDOT	PVA + 3 M LiCl + 2 M $ZnCl_2$ + 0.4 M $MnSO_4$	~1.4 V at 0.5 mA cm^{-2}	207.0 mAh g^{-1}	273.4 Wh kg^{-1}	41.8 Wh kg^{-1}	66
δ-NMOH	2 M $ZnSO_4$ + 0.2 M $MnSO_4$	~1.4 V at 380 mA g^{-1}	278 mAh g^{-1} at 380 mA g^{-1}	374 Wh kg^{-1} at 380 mA g^{-1}	–	67

[a] Note: without further clarification, the calculation is based on the total mass of the cell.

* Note: the cell energy density in this work is based on the total mass of the electrodeposited MnO_2, the carbon felt current collector, the zinc foil, all electrolytes and ion-exchange membranes.

** Note: the calculation is based on the condition that the content of cathode materials occupies one third of the whole weight of the battery[58,65].

*** Note: the calculation is based on the cathode and anode materials[61].

Abbreviations:

EG-waPUA/PAM: ethylene glycol based waterborne anionic polyurethane acrylates/polyacrylamide; PAAm: polyacrylamide; HPG: hydroponics polymer gel; CNT: carbon nanotube; PVA: polyvinyl alcohol; PEDOT: poly(3,4-ethylenedioxythiophene); ZHS: $Zn_4(OH)_6SO_4·5H_2O$; CNT HMs: carbon nanotubes hierarchically assembled microspheres; NFs: nanofibers; PANI: polyaniline; ZnHCF: zinc hexacyanoferrate; NC: N-doped carbon matrix; N-C: N-doped carbon; NG: N-doped graphene; rGO@HM-$ZnMn_2O_4$: graphene-wrapped hollow $ZnMn_2O_4$; ZVO: $Zn_3V_2O_7(OH)_2·2H_2O$; OD-ZMO: oxygen-deficient $ZnMn_2O_4$; δ-NMOH: Na ion and water molecule intercalated MnO_2 nanoplates.

Supplementary References

1. Chao, D. et al. An electrolytic Zn–MnO_2 battery for high-voltage and scalable energy storage. *Angew. Chem. Int. Ed.* **58,** 7823–7828 (2019).
2. Yadav, G.G., Turney, D., Huang, J., Wei, X. & Banerjee, S. Breaking the 2 V barrier in aqueous zinc chemistry: Creating 2.45 and 2.8 V MnO_2–Zn aqueous batteries. *ACS Energy Lett.* **4,** 2144–2146 (2019).
3. Liang, G. et al. A universal principle to design reversible aqueous batteries based on deposition–dissolution mechanism. *Adv. Energy Mater.* **9,** 1901838 (2019).
4. Lee, B. et al. Elucidating the intercalation mechanism of zinc ions into α-MnO_2 for rechargeable zinc batteries. *Chem. Commun.* **51,** 9265–9268 (2015).
5. Stoševski, I., Bonakdarpour, A., Cuadra, F. & Wilkinson, D.P. Highly crystalline ramsdellite as a cathode material for near-neutral aqueous MnO_2/Zn batteries. *Chem. Commun.* **55,** 2082–2085 (2019).
6. Su, S. et al. Holey nickel nanotube reticular network scaffold for high-performance flexible rechargeable Zn/MnO_2 batteries. *Chem. Eng. J.* **370,** 330–336 (2019).
7. Alfaruqi, M.H. et al. A high surface area tunnel-type α-MnO_2 nanorod cathode by a simple solvent-free synthesis for rechargeable aqueous zinc-ion batteries. *Chem. Phys. Lett.* **650,** 64–68 (2016).
8. Li, Y. et al. Reaction mechanisms for long-life rechargeable Zn/MnO_2 batteries. *Chem. Mater.* **31,** 2036–2047 (2019).
9. Ren, H. et al. Inverse opal manganese dioxide constructed by few-layered ultrathin nanosheets as high-performance cathodes for aqueous zinc-ion batteries. *Nano Res.* **12,** 1347–1353 (2019).
10. Huang, Y. et al. Novel insights into energy storage mechanism of aqueous rechargeable Zn/MnO_2 batteries with participation of Mn^{2+}. *Nano-Micro Lett.* **11,** 49 (2019).
11. Zhang, G.Q. & Zhang, X.G. A novel alkaline Zn/MnO_2 cell with alkaline solid polymer electrolyte. *Solid State Ionics* **160,** 155–159 (2003).
12. Wang, D. et al. A nanofibrillated cellulose/polyacrylamide electrolyte-based flexible and sewable high-performance Zn–MnO_2 battery with superior shear resistance. *Small* **14,** 1803978 (2018).
13. Alfaruqi, M.H. et al. Structural transformation and electrochemical study of layered MnO_2 in rechargeable aqueous zinc-ion battery. *Electrochim. Acta* **276,** 1–11 (2018).
14. Mo, F. et al. A flexible rechargeable aqueous zinc manganese-dioxide battery working at –20 °C. *Energy Environ. Sci.* **12,** 706–715 (2019).
15. Nam, K.W., Kim, H., Choi, J.H. & Choi, J.W. Crystal water for high performance layered manganese oxide cathodes in aqueous rechargeable zinc

batteries. *Energy Environ. Sci.* **12,** 1999–2009 (2019).
16. Chamoun, M., Brant, W.R., Tai, C.W., Karlsson, G. & Noréus, D. Rechargeability of aqueous sulfate Zn/MnO_2 batteries enhanced by accessible Mn^{2+} ions. *Energy Storage Mater.* **15,** 351–360 (2018).
17. Liu, Z. et al. A mechanically durable and device-level tough Zn-MnO_2 battery with high flexibility. *Energy Storage Mater.* **23,** 636–645 (2019).
18. Huang, Y., He, W., Zhang, P. & Lu, X. Nitrogen-doped MnO_2 nanorods as cathodes for high-energy Zn-MnO_2 batteries. *Funct. Mater. Lett.* **11,** 1840006 (2018).
19. Ismail, Y.M.B., Haliman, H. & Mohamad, A.A. Hydroponics polymer gels for Zn–MnO_2 alkaline batteries. *Int. J. Electrochem. Sci.* **7,** 3555–3566 (2012).
20. Qiu, W. et al. High-performance flexible quasi-solid-state Zn–MnO_2 battery based on MnO_2 nanorod arrays coated 3D porous nitrogen-doped carbon cloth. *J. Mater. Chem. A* **5,** 14838–14846 (2017).
21. Sun, G., Jin, X., Yang, H., Gao, J. & Qu, L. An aqueous Zn-MnO_2 rechargeable microbattery. *J. Mater. Chem. A* **6,** 10926–10931 (2018).
22. Wang, J., Wang, J.G., Liu, H., Wei, C. & Kang, F. Zinc ion stabilized MnO_2 nanospheres for high capacity and long lifespan aqueous zinc-ion batteries. *J. Mater. Chem. A* **7,** 13727–13735 (2019).
23. Sun, W. et al. Zn/MnO_2 battery chemistry with H^+ and Zn^{2+} coinsertion. *J. Am. Chem. Soc.* **139,** 9775–9778 (2017).
24. Minakshi, M., Singh, P., Carter, M. & Prince, K. The Zn-MnO_2 battery: The influence of aqueous LiOH and KOH electrolytes on the intercalation mechanism. *Electrochem. Solid-State Lett.* **11,** A145–A149 (2008).
25. Pan, H. et al. Reversible aqueous zinc/manganese oxide energy storage from conversion reactions. *Nat. Energy* **1,** 16039 (2016).
26. Poyraz, A.S., Laughlin, J. & Zec, Z. Improving the cycle life of cryptomelane type manganese dioxides in aqueous rechargeable zinc ion batteries: The effect of electrolyte concentration. *Electrochim. Acta* **305,** 423–432 (2019).
27. Palaniyandy, N. et al. α-MnO_2 nanorod/onion-like carbon composite cathode material for aqueous zinc-ion battery. *Mater. Chem. Phys.* **230,** 258–266 (2019).
28. Guo, C. et al. A case study of β- and δ-MnO_2 with different crystallographic forms on ion-storage in rechargeable aqueous zinc ion battery. *Electrochim. Acta* **324,** 134867 (2019).
29. Islam, S. et al. Facile synthesis and the exploration of the zinc storage mechanism of β-MnO_2 nanorods with exposed (101) planes as a novel cathode material for high performance eco-friendly zinc-ion batteries. *J. Mater. Chem. A* **5,** 23299–23309 (2017).
30. Deng, Z. et al. β-MnO_2 nanolayer coated on carbon cloth as a high-activity aqueous zinc-ion battery cathode with high-capacity and long-cycle-life. *Mater. Lett.* **248,** 207–210 (2019).
31. Guo, C. et al. Ultrathin δ-MnO_2 nanosheets as cathode for aqueous rechargeable zinc ion battery. *Electrochim. Acta* **304,** 370–377 (2019).
32. Wang, K. et al. High-performance cable-type flexible rechargeable Zn battery based on MnO_2@CNT fiber microelectrode. *ACS Appl. Mater. Interfaces* **10,** 24573–24582 (2018).
33. Zhao, L., Dong, L., Liu, W. & Xu, C. Binary and ternary manganese dioxide composites cathode for aqueous zinc-ion battery. *ChemistrySelect* **3,** 12661–12665 (2018).

34. Gou, L. et al. α-MnO_2@In_2O_3 nanotubes as cathode material for aqueous rechargeable Zn-ion battery with high electrochemical performance. *J. Electrochem. Soc.* **166,** A3362–A3368 (2019).
35. Zeng, Y. et al. Achieving ultrahigh energy density and long durability in a flexible rechargeable quasi-solid-state Zn–MnO_2 battery. *Adv. Mater.* **29,** 1700274 (2017).
36. Zhao, S. et al. Unravelling the reaction chemistry and degradation mechanism in aqueous Zn/MnO_2 rechargeable batteries. *J. Mater. Chem. A* **6,** 5733–5739 (2018).
37. Islam, S. et al. Carbon-coated manganese dioxide nanoparticles and their enhanced electrochemical properties for zinc-ion battery applications. *J. Energy Chem.* **26,** 815–819 (2017).
38. Liu, Y. et al. α-MnO_2 nanofibers/carbon nanotubes hierarchically assembled microspheres: Approaching practical applications of high-performance aqueous Zn-ion batteries. *J. Power Sources* **443,** 227244 (2019).
39. Wang, C. et al. *γ*-MnO_2 nanorods/graphene composite as efficient cathode for advanced rechargeable aqueous zinc-ion battery. *J. Energy Chem.* **43,** 182–187 (2020).
40. Khamsanga, S., Pornprasertsuk, R., Yonezawa, T., Mohamad, A.A. & Kheawhom, S. δ-MnO_2 nanoflower/graphite cathode for rechargeable aqueous zinc ion batteries. *Sci. Rep.* **9,** 8441 (2019).
41. Zhang, X. et al. 3D CNTs networks enable MnO_2 cathodes with high capacity and superior rate capability for flexible rechargeable Zn–MnO_2 batteries. *Small Methods* **3,** 1900525 (2019).
42. Wu, B. et al. Graphene scroll-coated *α*-MnO_2 nanowires as high-performance cathode materials for aqueous Zn-Ion battery. *Small* **14,** 1703850 (2018).
43. Alfaruqi, M.H. et al. A layered δ-MnO_2 nanoflake cathode with high zinc-storage capacities for eco-friendly battery applications. *Electrochem. Commun.* **60,** 121–125 (2015).
44. Yuan, T. et al. Novel alkaline Zn/$Na_{0.44}MnO_2$ dual-ion battery with a high capacity and long cycle lifespan. *ACS Appl. Mater. Interfaces* **10,** 34108–34115 (2018).
45. Xiong, T. et al. Defect engineering of oxygen-deficient manganese oxide to achieve high-performing aqueous zinc ion battery. *Adv. Energy Mater.* **9,** 1803815 (2019).
46. Huang, J. et al. Polyaniline-intercalated manganese dioxide nanolayers as a high-performance cathode material for an aqueous zinc-ion battery. *Nat. Commun.* **9,** 2906 (2018).
47. Lu, K., Song, B., Zhang, Y., Ma, H. & Zhang, J. Encapsulation of zinc hexacyanoferrate nanocubes with manganese oxide nanosheets for high-performance rechargeable zinc ion batteries. *J. Mater. Chem. A* **5,** 23628–23633 (2017).
48. Liu, G. et al. K^+ pre-intercalated manganese dioxide with enhanced Zn^{2+} diffusion for high rate and durable aqueous zinc-ion batteries. *J. Mater. Chem. A* **7,** 20806–20812 (2019).
49. Bischoff, C. et al. Investigating the impact of particle size on the performance and internal resistance of aqueous zinc ion batteries with a manganese sesquioxide cathode. *Batteries* **4,** 44 (2018).
50. Jiang, B. et al. Manganese sesquioxide as cathode material for multivalent zinc ion battery with high capacity and long cycle life. *Electrochim. Acta* **229,**

422–428 (2017).

51. Wang, L., Cao, X., Xu, L., Chen, J. & Zheng, J. Transformed akhtenskite MnO_2 from Mn_3O_4 as cathode for a rechargeable aqueous zinc ion battery. *ACS Sustainable Chem. Eng.* **6,** 16055–16063 (2018).
52. Hao, J. et al. Electrochemically induced spinel-layered phase transition of Mn_3O_4 in high performance neutral aqueous rechargeable zinc battery. *Electrochim. Acta* **259,** 170–178 (2018).
53. Chen, H. et al. Porous cube-like Mn_3O_4@C as an advanced cathode for low-cost neutral zinc-ion battery. *J. Alloy. Compd.* **813,** 15812 (2020).
54. Sun, M. et al. Mn_3O_4@NC composite nanorods as a cathode for rechargeable aqueous Zn-ion batteries. *ChemElectroChem* **6,** 2510–2516 (2019).
55. Fu, Y. et al. High-performance reversible aqueous Zn-ion battery based on porous MnO_x nanorods coated by MOF-derived N-doped carbon. *Adv. Energy Mater.* **8,** 1801445 (2018).
56. Soundharrajan, V. et al. Aqueous magnesium zinc hybrid battery: An advanced high-voltage and high-energy $MgMn_2O_4$ cathode. *ACS Energy Lett.* **3,** 1998–2004 (2018).
57. Wu, X. et al. Green-low-cost rechargeable aqueous zinc-ion batteries using hollow porous spinel $ZnMn_2O_4$ as the cathode material. *J. Mater. Chem. A* **5,** 17990–17997 (2017).
58. Zhang, N. et al. Cation-deficient spinel $ZnMn_2O_4$ cathode in $Zn(CF_3SO_3)_2$ electrolyte for rechargeable aqueous Zn-ion battery. *J. Am. Chem. Soc.* **138,** 12894–12901 (2016).
59. Yang, S. et al. The excellent electrochemical performances of $ZnMn_2O_4/Mn_2O_3$: The composite cathode material for potential aqueous zinc ion batteries. *J. Electroanal. Chem.* **832,** 69–74 (2019).
60. Chen, L., Yang, Z., Qin, H., Zeng, X. & Meng, J. Advanced electrochemical performance of $ZnMn_2O_4$/N-doped graphene hybrid as cathode material for zinc ion battery. *J. Power Sources* **425,** 162–169 (2019).
61. Yan, L. et al. An innovation: Dendrite free quinone paired with $ZnMn_2O_4$ for zinc ion storage. *Mater. Today Energy* **13,** 323–330 (2019).
62. Chen, L. et al. Graphene-wrapped hollow $ZnMn_2O_4$ microspheres for high-performance cathode materials of aqueous zinc ion batteries. *Electrochim. Acta* **317,** 155–163 (2019).
63. Guo, J. et al. Artificial solid electrolyte interphase for suppressing surface reactions and cathode dissolution in aqueous zinc ion batteries. *ACS Energy Lett.* **4,** 2776–2781 (2019).
64. Fang, G. et al. Suppressing manganese dissolution in potassium manganate with rich oxygen defects engaged high-energy-density and durable aqueous zinc-ion battery. *Adv. Funct. Mater.* **29,** 1808375 (2019).
65. Long, J. et al. Highly porous, low band-gap $Ni_xMn_{3-x}O_4$ ($0.55 \leq x \leq 1.2$) spinel nanoparticles with *in situ* coated carbon as advanced cathode materials for zinc-ion batteries. *J. Mater. Chem. A* **7,** 17854–17866 (2019).
66. Zhang, H. et al. Extracting oxygen anions from $ZnMn_2O_4$: Robust cathode for flexible all-solid-state Zn-ion batteries. *Energy Storage Mater.* **21,** 154–161 (2019).
67. Wang, D. et al. A superior δ-MnO_2 cathode and a self-healing Zn-δ-MnO_2 battery. *ACS Nano* **13,** 10643–10652 (2019).